Chalmers University of Technology (2025) TR-2025-1.
doi: 10.63959/m2.techreport/2025.1

Hybrid Parameterization of Symmetrically Cambered (Crescent-Shaped) Airfoil Profiles for Rigid Wingsail Design in Wind-Assisted Ship Propulsion

March 1, 2025

Hua-Dong Yao

Department of Mechanics and Maritime Sciencies,
Chalmers University of Technology,
Gothenburg, SE-41296, Sweden

Abstract

Wind-assisted ship propulsion (WASP) is increasingly recognized as a viable pathway to enhance the efficiency and sustainability of maritime transport. Rigid wingsails with symmetrically cambered (SC), thick (crescent-shaped) profiles offer superior aerodynamic performance, but their complex geometries necessitate effective parameterization to support efficient aerodynamic and aero-structural design optimization. This paper presents and compares four parameterization methods for constructing SC profiles, as well as a U-shaped profile from the literature. The first method from the previous work uses circular arcs that provide geometric simplicity. The second method proposed by us derives profiles from classical NACA series, while the third one is completely based on Bézier curves that enable flexible and smooth geometric adjustments. Lastly, a hybrid method is proposed by combining the modified NACA series for thickness distribution with the second method for camber line adjustment. These methods form the basis of a framework that balances fidelity and adaptability in airfoil profile parameterization, and support future multidisciplinary design optimization of SC rigid wingsails.

Keywords: airfoil profile, crescent-shaped, geometric parameterization, rigid wingsail, symmetrically cambered, wind assisted ship propulsion

Chalmers University of Technology (2025) TR-2025-1.
doi: 10.63959/m2.techreport/2025.1

1. Introduction

Wind-assisted ship propulsion (WASP) has emerged as a promising approach to enhance the efficiency and sustainability of maritime transport (Thies and Ringsberg, 2025). By utilizing sails, kites or other aerodynamic devices, WASP can capture wind energy to supplement the vessel's primary propulsion system or even act as the primary propulsor. This leads to not only significant fuel savings and decreased greenhouse gas emissions, but also promotes the use of renewable energy (Arabnejad et al., 2024).

Rigid wingsails designed with symmetrically cambered (SC), also termed crescent-shaped, sectional profiles have shown great potential for WASP because the aerodynamics is enhanced by the camber. SC wingsails installed on a large cargo vessel, "Wind Challenger", were developed by Ouchi et al. (2011, 2013). A U-shaped wingsail configuration was presented by Chen et al. (2019), which could essentially be categorized into CS wingsails. Later, the tanker New Vitality, equipped with two U-shaped sails, was deployed in 2018, followed by its sister tanker New Aden, which carried four such sails, in 2022 (Zhang et al., 2023). On the other hand, SC wingsails for large commercial vessels, initially designed by ScandiNAOS AB in the 1990s, were investigated to understand the aerodynamics and aeroelastics through computational fluid dynamics (CFD), finite element analysis (FEA) and model-scale wind tunnel tests (Nikmanesh, 2021; Zhu et al., 2022, 2023, 2024). Meanwhile, a similar geometry of the sectional profile was also reported in a patent (Zeng et al., 2011), and another similar geometry composed of Bézier curves created by us was investigated (van Reen et al., 2025).

However, the sectional profiles of the SC wingsails surveyed above are geometrically different, despite the common features such as the overall symmetry about the axis normal to the chord, varying thickness distribution along the chord, and the non-zero camber height. There is no doubt that an SC profile can be defined in various ways by parameterizing its geometry, with the choice of approach guided by the experience and design perspective of the engineer or scientist. Therefore, it is interesting to overview the profiles that have been available in the literature, and propose several new ideas for parameterization, which are expected to stimulate both fundamental research and practical engineering applications. In particular, these methods can be used for aerodynamics or aero-structural optimization.

Email address: huadong.yao@chalmers.se (Hua-Dong Yao)

Chalmers University of Technology (2025) TR-2025-1.
doi: 10.63959/m2.techreport/2025.1

In this paper, four parameterization methods (Methods 1–4) will be presented. Method 1 was proposed by ScandiNAOS AB, and the other methods are newly developed by us. Lastly, an existing geometry (Design 5) from Chen et al. (2019) will be briefly described, as the method of parameterizing this geometry is not available in the open literature.

2. Method 1 – circular arc segments

An original parameterization method for generating SC airfoil profiles for rigid wingsails was proposed by ScandiNAOS AB in Sweden in the 1990s, while it was not documented in the open literature but mainly developed within national research and commercial projects. The method was published until the work by Nikmanesh (2021); Zhu et al. (2022, 2023, 2024), where the aerodynamics of this type of profile was systematically investigated. Meanwhile, a similar profile was briefly sketched by Zeng et al. (2011), but there are also no public documents that report the parameterization method and subsequent work for this profile. Nevertheless, it is worth noting that another profile has been patented and well studied by Chinese researchers in recent years, which will be described as Design 5 in the next section.

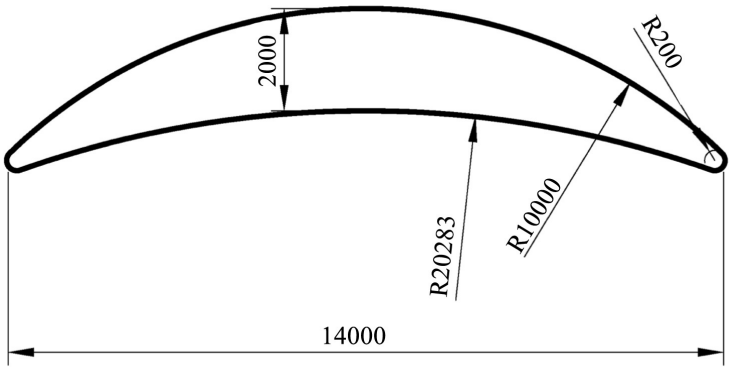

Figure 1: Parameterization of symmetrically-cambered wingsail profile in Method 1 proposed by ScandiNAOS AB. The unit of all numbers is mm, and "R" denotes the radius. Reproduced from Zhu et al. (2023).

An example of the profiles is shown in Fig. 1, which was found with the best aerodynamic performance in a set of profiles generated using this method (Nikmanesh, 2021; Zhu et al., 2022). The profile consists of four curve

segments: two circular arcs symmetrically designated to form the leading and trailing edges, one circular arc for the pressure side of the profile (the bottom side in Fig. 1), and one circular arc for the suction side (the top side in the figure). Since all of these arcs are circular, it is straightfoward to ensure tangency at their junctions. The maximum thickness of the profile, that is, the maximum distance between the top and bottom arcs, is determined with the diameter of the sail mast. The length of the chord is counted between the two extreme points of the profile, rather than the centers of the two small circles. This suggests that the chord length is dependent on the radii of the arcs at the leading and trailing edges. Therefore, there are three design parameters in the profile definition, such as the radius of the two edge arcs, that of the top arc, and that of the bottom arc.

As illustrated in Fig. 1, ScandiNAOS AB chose 14 m for the chord length of a real wingsail. The maximum thickness of 2 m in order to accomendate the sail mast. The aerodynamics of this profile have been investigated by the authors (Nikmanesh, 2021; Zhu et al., 2022, 2023, 2024), as well as some preliminary studies of its aeroelastics.

The parameterization based on circular arcs was also investigated by Guzelbulut et al. (2024) for aerodynamic optimization, as shown in Fig. 2. Here, the drawing highlights the circular arcs for constructing the camber line, the leading and traiding edges, and the bottom suction-side curve. The radii of these circular arcs are labeled as R_1, R_2, and R_3, respectively. Although these parameters are different from those defined by ScandiNAOS AB (the difference is that the top arc instead of the camber line is set), the two methods are essentially the same. The basic principle is illustrated in Fig. 3. Once the lower circular arc and the location of maximum thickness (indicated by the dashed circles) are established, specifying either the camber line or the upper circular arc becomes equivalent.

3. Method 2 – mirroring rear part of NACA-series profile

Airfoil geometries developed by the National Advisory Committee for Aeronautics (NACA) in the early 20th century marked a significant advancement in aerodynamic design (Jacobs et al., 1933). The 4-digit NACA series was the first widely used formulation. In this notation, each digit specifies a geometric characteristic of the camber line and thickness distribution. The name NACA *MPXX* encodes the defining geometric parameters of the airfoil. Specifically, the first digit M gives the maximum camber as a percentage of

Chalmers University of Technology (2025) TR-2025-1.
doi: 10.63959/m2.techreport/2025.1

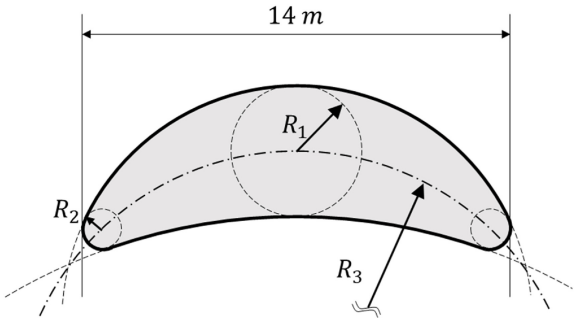

Figure 2: The SC wingsail profile composed of circular arcs. Reproduced from Guzelbulut et al. (2024).

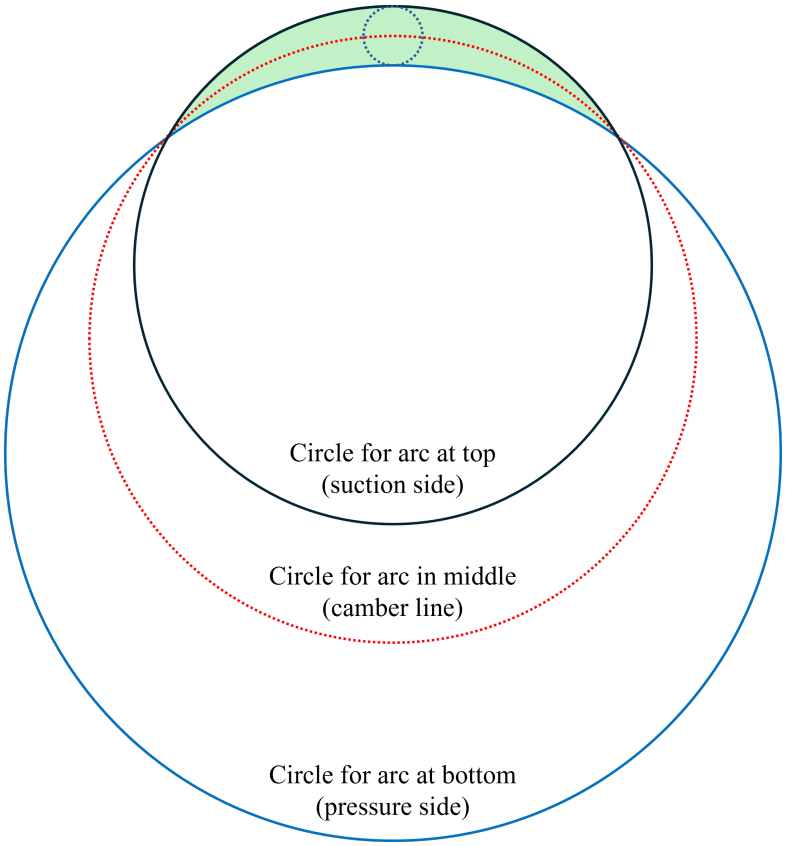

Figure 3: Basic circular arcs constituting an SC profile based on the principles of Method 1. The actual profile region is colored in green.

chord. The second digit P specifies the chordwise position of the maximum camber in tenths of the chord. The last two digits XX denote the maximum thickness as a percentage of the chord. For example, the NACA 2315 airfoil has a maximum camber of 2% located at 30% of the chord from the leading edge, with a maximum thickness of 15% of the chord length.

The thickness distribution of a NACA 4-digit airfoil is expressed as (Mason, 2018):

$$\frac{y_t(x)}{c} = 5\left(\frac{h_t}{c}\right)\left[a_0\sqrt{\frac{x}{c}} + a_1\left(\frac{x}{c}\right) + a_2\left(\frac{x}{c}\right)^2 + a_3\left(\frac{x}{c}\right)^3\right], \quad 0 \le \frac{x}{c} \le 1 \quad (1)$$

where h_t is the maximum thickness. The coefficients are specified as:

$$\begin{aligned} &a_0 = 0.2969, \quad a_1 = -0.1260, \quad a_2 = -0.3516, \quad a_3 = 0.2843, \\ &a_4 = -0.1036 \text{ or } -0.1015. \end{aligned} \quad (2)$$

Setting $a_4 = -0.1036$ leads to a closed training edge (i.e., $y_t = 0$ at $x/c = 1$), whereas -0.1015 results in a finite thickness at this position.

In the present work, $a_4 = -0.1036$ is chosen to construct the SC profile, so that the curve is closed at the trailing edge. This is to achieve an extreme case where the trailing and leading edges are sharp instead of blunt.

In the NACA 4-digit series, the thickness distribution function is fixed, since the polynomial coefficients are not adjustable. This means the shape of the thickness distribution is the same for all NACA 4-digit airfoils, only scaled by the maximum thickness parameter h_t. Because of this, the position of the maximum thickness is always the same fraction of the chord as $x/c \approx 0.3$. Beyond the 4-digit series, more advanced formulations were developed, such as the modified 4-digit, 5-digit (optimized for higher lift coefficients) and 6-digit series (designed to achieve favorable laminar flow characteristics) (Mason, 2018). These subsequent generations of NACA airfoils introduced modified thickness distributions where the maximum thickness location can shift (e.g., toward $x/c = 0.4$ or 0.5) to improve laminar flow characteristics. They reflected a shift from purely geometric parameterizations to designs informed by aerodynamic performance requirements.

The height distribution of the camber line for a classical NACA 4-digit

airfoil is generally expressed as:

$$\frac{y_c(x)}{c} = \begin{cases} \dfrac{h_c}{c}\left[2\dfrac{x}{x_c} - \left(\dfrac{x}{x_c}\right)^2\right], & 0 \le x \le x_c, \text{ (a)} \\ \dfrac{h_c}{c}\dfrac{1}{(c/x_c - 1)^2}\left[\left(\dfrac{c}{x_c}\right)^2 - 2\dfrac{c}{x_c} + 2\dfrac{x}{x_c} - \left(\dfrac{x}{x_c}\right)^2\right], & x_c < x \le c, \text{ (b)} \end{cases} \tag{3}$$

where h_c denotes the maximum camber height, c the chord length, and x_c the chordwise coordinate of the maximum thickness. The leading edge is at $x = 0$, and the trailing edge at $x = c$.

The profile is shaped by superimposing the thickness with the camber height. Given the maximum thickness at $x/c = 0.3$, the maximum camber height is also set at the same position. That is, h_c at $x_c = 0.3c$.

At $x/c = 0.3$, the chordwise gradients of the thickness change signs along the chord. This means that the thickness transitions from an increasing trend to a decreasing one. It is reasonable to split the profile into two parts at this position. The rear part is used to generate half of the SC profile.

To blunt the trailing edge of the rear part, a circular arc is introduced. The center of the arc is positioned in the camber line. The arc parameters, the center position and angular extent, are selected such that tangential continuity is satisfied at the junctions with the pressure- and suction-side curves. This requires to first calculate local tangencies near the truncated ends of the pressure- and suction-side curves, and then derive the parameters for the arc accordingly.

Once the rear part is blunted, it is mirrored about the axis normal to the chord at the splitting position of $x/c = 0.3$, to generate the front part. The blunting treatment leads to an offset of the ending point from the original position $x = 1$. The chord should be scaled to a constant value, such as c, so that different profiles can be compared on the same length. An example of the profile constructed using Method 2 is shown in Fig. 4.

4. Method 3 – Bézier curve segments

The mathematical framework of Bézier curves was introduced into engineering design practice by Pierre Bézier (1910–1999) during the 1960s. In general, a Bézier curve of degree n is defined over the parameter domain

Chalmers University of Technology (2025) TR-2025-1.
doi: 10.63959/m2.techreport/2025.1

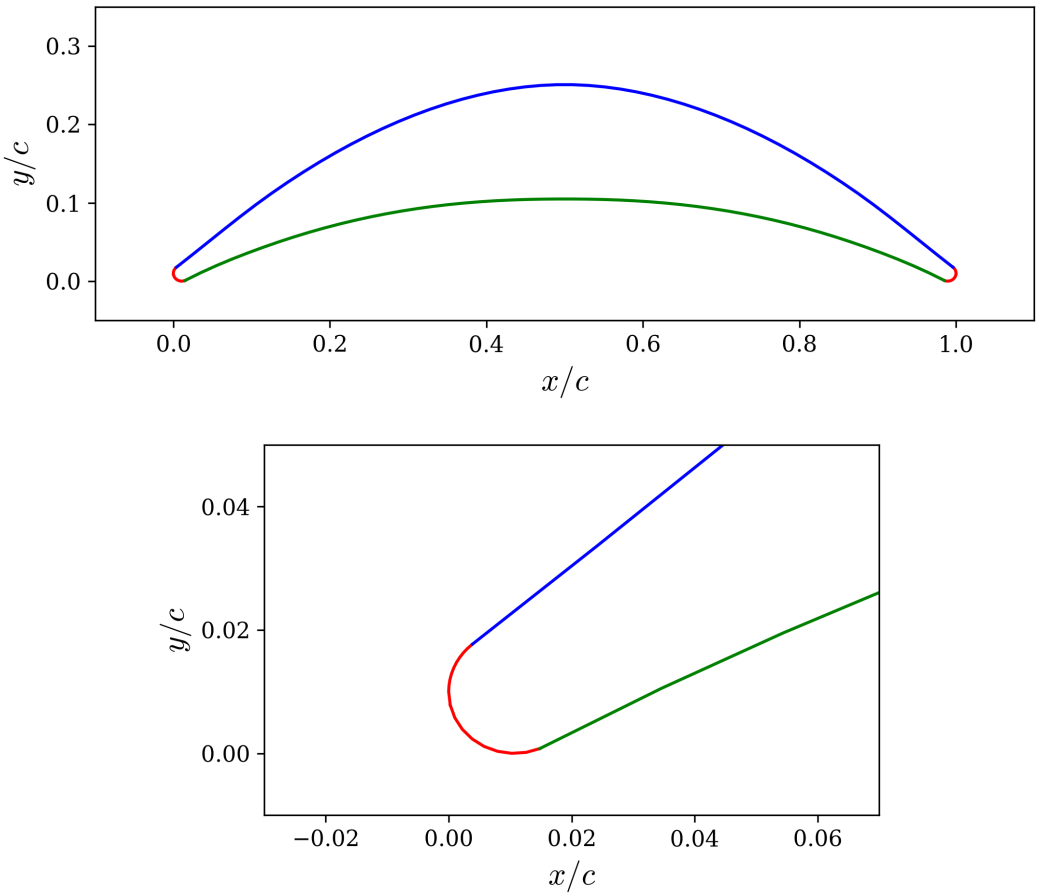

Figure 4: The SC profile based on classical NACA 4-digit series using Method 2: overview (top) and zoom-in view near the leading edge (bottom).

$t \in [0, 1]$ as:

$$B(t) = \sum_{i=0}^{n} b_{i,n}(t) P_i, \tag{4}$$

where P_i are the control points, and $b_{i,n}(t)$ are the Bernstein basis polynomials:

$$b_{i,n}(t) = \binom{n}{i} (1-t)^{n-i} t^i. \tag{5}$$

This representation guarantees several desirable properties. The curve is contained within the convex hull of its control points. It is affine invariant

under translation, rotation, and scaling. And it exhibits smooth continuity with well-defined tangents at the endpoints.

Depending on the polynomial degree, Bézier curves may be linear, quadratic, cubic, or higher order. The cubic Bézier curve, defined by four control points, is particularly prevalent due to its balance of computational efficiency and geometric expressiveness. It takes the form:

$$B(t) = (1-t)^3 P_0 + 3(1-t)^2 t P_1 + 3(1-t)t^2 P_2 + t^3 P_3, \quad t \in [0,1]. \tag{6}$$

Beyond single curve segments, Bézier curves can be concatenated to form Bézier splines, enabling the representation of more complex geometries while maintaining smooth continuity across segment boundaries. The concept also generalizes naturally into higher dimensions, yielding Bézier surfaces that are widely used in three-dimensional modeling.

In the present work, nine Bézier curve segments are used to define the front half of the profile, as shown in Fig. 5. To facilitate design optimization, a benchmark profile should be defined beforehand, for which Method 2 is used. The Bézier curve segments are optimized by adjusting their control points so that they accurately coincide with the corresponding curves of the benchmark profile, except for the region near the leading edge where two control points are vertically aligned to control the bluntness. Meanwhile, the two segments adjacent to the symmetry axis are constrained to have zero gradient at the axis. Under the constraints, the complete geometry is constructed by mirroring the curve segments of the front half part.

5. Method 4 – hybrid NACA and Bézier curves

Methods 2 and 3 can be combined to formulate a hybrid method that inherits features and advantages of both methods. NACA series foils and cambers are used as reference components, and curvature definition with Bézier curves provides greater freedom to explore potential high-performance geometries.

Firstly, a reference camber line is derived from NACA 4-digit series. Its definition follows the front part upstream of the position of the maximum camber height prescribed in Eq. 3(a). Since the camber line is symmetric, the maximum camber position is set to $x_c/c = 0.5$. By mirroring the half line, the complete camber has the height distribution as:

$$\frac{y_c}{c} = \frac{4h_c}{c}\left[\frac{x}{c} - \left(\frac{x}{c}\right)^2\right], \quad 0 \le \frac{x}{c} \le 1\,, \tag{7}$$

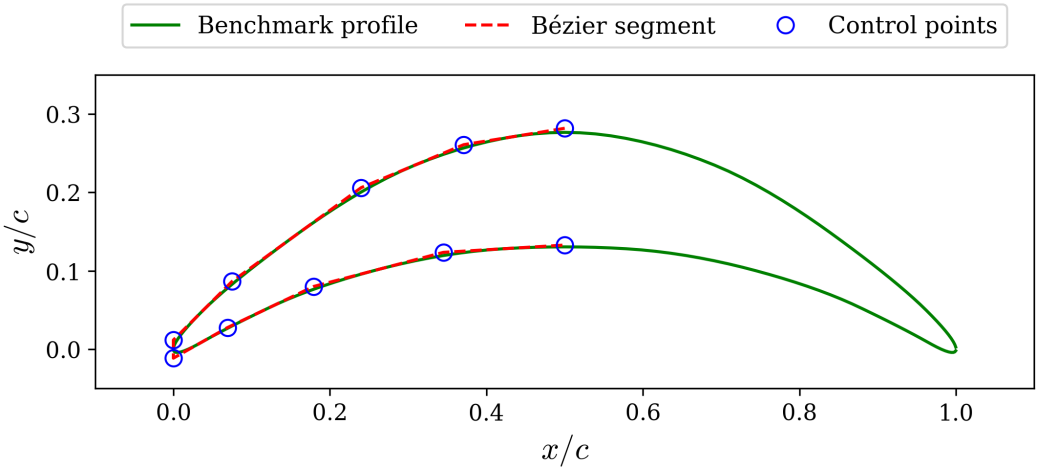

Figure 5: The benchmark profile fitted with Bézier curve segments using Method 3.

for which h_c is the only parameter needing to be specified.

A symmetric Bézier curve for defining the camber is generated by fitting it to the reference camber line defined in Eq. 7. As shown in Fig. 6, five control points are used to shape a Bézier curve. Through an optimization technique, the curve that best matches the reference camber line can be obtained. It is also possible to employ more control points to get more flexible adjustment in practice, despite the five control points used in the present work.

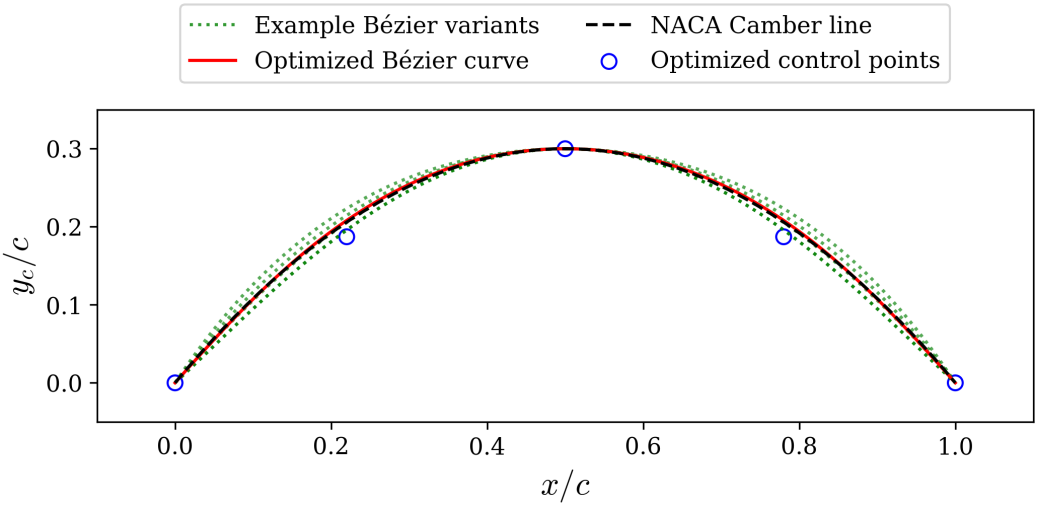

Figure 6: The Bézier camber line derived from the NACA reference in Method 4.

In the next step, the profile thickness is prescribed based on the front half of a profile from the modified NACA 4-digit series (Mason, 2018). The thickness distribution is also governed by Eq. 1. However, the coefficients in the equation are changed for the modified NACA 4-digit series. The changes enable the maximum thickness to be positioned at the middle of the chord. Thus, Method 4 adopts the chordwise coordinate of $0 \leq x/c \leq 0.5$ for the front half part.

The coefficient a_0 changed for the modified NACA 4-digit series is:

$$a_0 \approx 0.296904 \cdot \chi_{LE}\,, \tag{8}$$

and

$$\chi_{LE} = \begin{cases} I/6\,, & \text{for } I \leq 8 \\ 10.3933\,, & \text{for } I = 9 \end{cases} \tag{9}$$

where I denotes the bluntness index, which characterizes the leading-edge curvature. The other coefficients are as follows:

$$a_1 \approx 0.477 - 2.650a_0 \tag{10}$$

$$a_2 \approx -0.708 + 3.536a_0 \tag{11}$$

$$a_3 \approx 0.308 - 2.121a_0 \tag{12}$$

According to Eqs. 1 and 8-12, the thickness distribution is parameterized with the maximum thickness h_t and the bluntness index I. By mirroring the front half part about the vertical axis at $x/c = 0.5$, the rear half part is generated. An example derived from the modified NACA 16-series profile with $h_t = 0.16c$ and $I = 6$ is shown in Fig. 7, where the classical NACA 0016 profile is also compared.

By superimposing the Bézier camber and the modified NACA thickness, an SC profile is constructed. An example is illustrated in Fig. 8. Here the front half of the modified NACA 16-series profile with $h_t = 0.16c$ and $I = 6$ is used for the construction.

6. Design 5 – U-shaped profile

The U-shaped profile was developed by the China Shipbuilding Industry Corporation (CSIC) (Zhang et al., 2023), and its geometry can be found in the work by Chen et al. (2019). The geometry of this profile is shown in

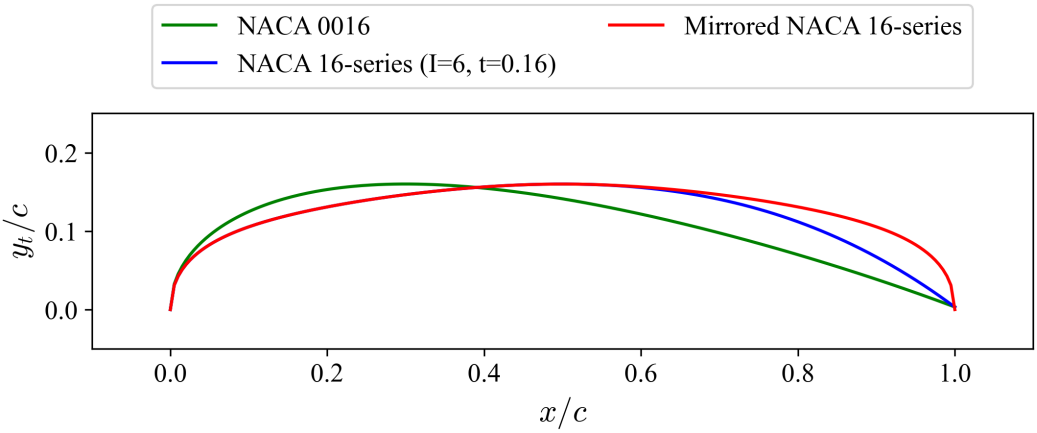

Figure 7: The thickness distribution (in red) derived from the NACA 16-series profile with $h_t = 0.16c$ and $I = 6$ (in blue) using Method 4, and compared to the classical NACA 0016 profile (in green).

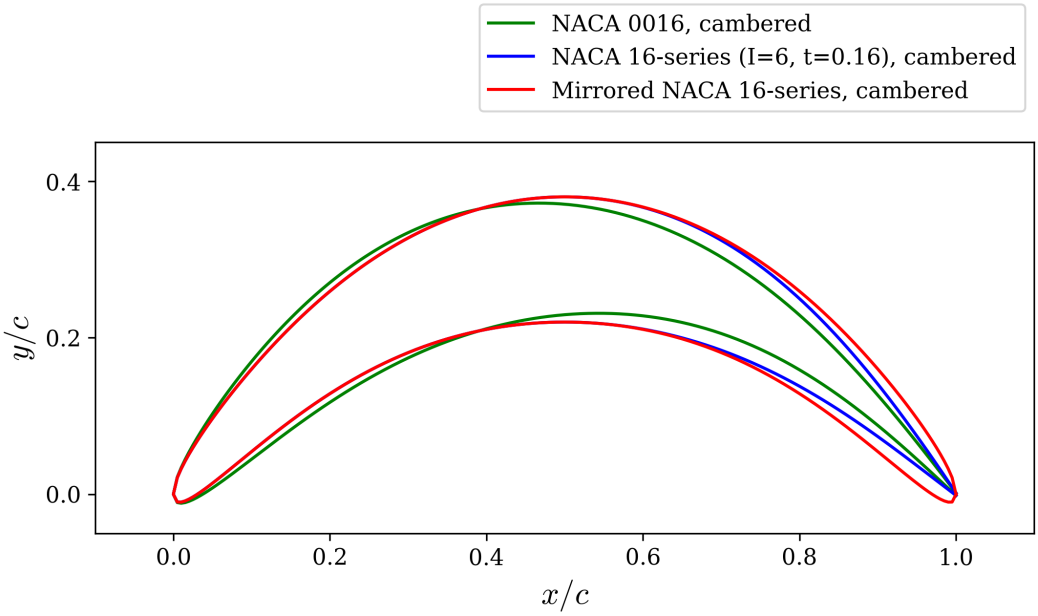

Figure 8: The SC profile (in red) derived from the NACA 16-series profile with $h_t = 0.16c$ and $I = 6$ (in blue) using Method 4, and compared to the classical NACA 0016 profile that is imposed with the same camber (in green).

Fig. 9. Rigid wingsails with the profile have been deployed on the tankers New Vitality and New Aden, constructed by Dalian Shipbuilding Industry

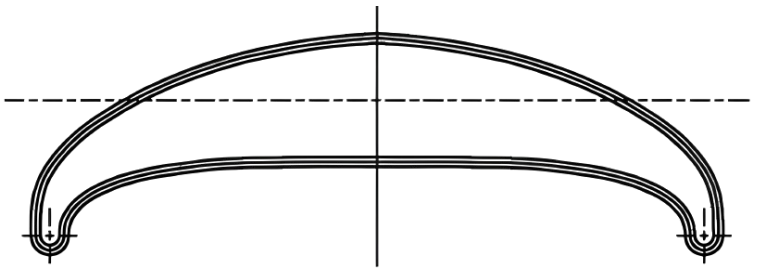

Figure 9: The U-shape profile. Reproduced from Chen et al. (2019).

Co., Ltd. (DSIC) and currently operated by China Merchants Energy Shipping Co., Ltd. (Zhang et al., 2023).

The parameterization method of this profile has not been reported in the open literature. But it is still interesting to learn the profile based on the diagram. Instead of categorizing the method, the profile is termed Design 5 in the present paper.

7. Summary

This paper presents a comparative overview of geometric parameterization methods for symmetrically cambered (SC), crescent-shaped airfoil profiles that are used to design rigid wingsails in wind-assisted ship propulsion.

Four parameterization approaches are discussed. Method 1, developed by ScandiNAOS AB, constructs the profile from circular arc segments, featuring geometric simplicity and straightforward tangency enforcement. Method 2 mirrors the rear half part of a classical NACA 4-digit airfoil about the position of the maximum thickness. It leverages a well-established aerodynamic shape. Method 3 adopts a fully parametric approach using Bézier curve segments. Thus, it provides flexible and smooth geometric control. Hybrid Method 4 combines a modified NACA 4-digit thickness distribution with a Bézier-based camber line. This method balances the robustness of classical profiles with the adaptability of free-form parameterization. Additionally, an existing U-shaped profile (Design 5) from industry is described, although its parameterization remains undocumented in the open literature.

These methods form a flexible framework for generating SC airfoil profiles, catering to different design priorities ranging from simplicity and robustness to high flexibility for multidisciplinary design optimization. This work provides a foundation for future studies aimed at optimizing the aerodynamic

and structural performance of rigid wingsails.

Acknowledgment

This research was carried out in the project "generic multidisciplinary optimization for sail installation on wind-assisted ships (GEMINI)" funded by the Swedish Transport Administration. The computations and data handling were enabled by resources provided by the National Academic Infrastructure for Supercomputing in Sweden (NAISS), partially funded by the Swedish Research Council through grant agreement no. 2022-06725.

References

Arabnejad, M.H., Thies, F., Yao, H.D., Ringsberg, J.W., 2024. Zero-emission propulsion system featuring flettner rotors, batteries and fuel cells, for a merchant ship. Ocean Engineering 310, 118618. doi:10.1016/j.oceaneng.2024.118618.

Chen, L., Zhang, Q., Hou, Y., Peng, G., Xu, H., Jiang, Z., Wang, S., Wang, J., Li, W., Wang, K., Zhao, X., Wang, Q., Zhang, Q., 2019. Skeleton cross-type sail. Invention Patent Publication, CN109677581A, Dalian Shipbuilding Industry Co., Ltd.

Guzelbulut, C., Badalotti, T., Suzuki, K., 2024. Optimization techniques for the design of crescent-shaped hard sails for wind-assisted ship propulsion. Ocean Engineering 312, 119142. doi:https://doi.org/10.1016/j.oceaneng.2024.119142.

Jacobs, E.N., Ward, K.E., Pinkerton, R.M., 1933. The characteristics of 78 related airfoil sections from tests in the variable-density wind tunnel. Research report 460. National Advisory Committee for Aeronautics.

Mason, W.H., 2018. Configuration Aerodynamics. Virginia Tech, Blackburg VA.

Nikmanesh, M., 2021. Sailing performance analysis using CFD simulations: A study on crescent shaped wing profiles. Master's thesis. Chalmers University of Technology. Gothenburg.

Ouchi, K., Uzawa, K., Kanai, A., 2011. Huge hard wing sails for the propulsor of next generation sailing vessel, in: Second International Symposium on Marine Propulsors, Hamburg, Germany.

Ouchi, K., Uzawa, K., Kanai, A., Katori, M., 2013. Wind challenger: The next generation hybrid sailing vessel, in: Third International Symposium on Marine Propulsors smp'13, Launceston, Tasmania, Australia, May 2013.

van Reen, S., Zhu, H., Lin, J., Niu, J., Sharpe, P., Yao, H.D., 2025. Aerodynamic optimization of in-line and parallel layouts for symmetric cambered wingsail installation. Proceedings of the ASME 2025 44th International Conference on Ocean, Offshore and Arctic Engineering (OMAE 2025) , OMAE2025–155321.

Thies, F., Ringsberg, J.W., 2025. Sea trials vs prediction by numerical models—uncertainties in the measurements and prediction of WASP performance. Journal of Ocean Engineering and Science 10, 239–245. doi:10.1016/j.joes.2024.05.001.

Zeng, X., Hu, Y., Su, F., Chen, L., Wang, H., Huang, X., Li, S., 2011. Elliptical arc sail. Utility Model Patent, CN201745736U, Shanghai Maritime University.

Zhang, R., Huang, L., Peng, G., Ma, R., Wang, K., Tian, F., Song, Q., 2023. A novel method of desynchronized operation of sails for ship wind-assisted propulsion system. Ocean Engineering 288, 115964. doi:10.1016/j.oceaneng.2023.115964.

Zhu, H., Nikmanesh, M., Yao, H.D., Ramne, B., Ringsberg, J., 2022. Propulsive performance of a novel crescent-shaped wind sail analyzed with unsteady rans in 2D and 3D. Proceedings of the ASME 2022 41st International Conference on Ocean, Offshore and Arctic Engineering (OMAE 2022), Hamburg, Germany , OMAE2022–79867.

Zhu, H., Yao, H.D., Ringsberg, J.W., 2024. Unsteady RANS and IDDES studies on a telescopic crescent-shaped wingsail. Ships and Offshore Structures 19, 134–147. doi:10.1080/17445302.2023.2256601.

Zhu, H., Yao, H.D., Thies, F., Ringsberg, J., Ramne, B., 2023. Propulsive performance of a rigid wingsail with crescent-shaped profiles. Ocean Engineering 285, part 2, 115349. doi:10.1016/j.oceaneng.2023.115349.